Calculated hybrid and semilocal functionals and *GW* electronic structure of the metal trifluorides MF_3 (*M*=Sc, Y, Al)

Hichem Ben Hamed,[1,2] A. Qteish,[3,4] N. Meskini,[2] and M. Alouani[1]

[1]*Institut de Physique et de Chimie des Matériaux de Strasbourg (IPCMS), UMR 7504 du CNRS, 23 rue du Loess, 67034 Strasbourg, France*

[2]*Département de Physique, Faculté des Sciences de Tunis, Université Tunis El Manar, Campus Universitaire, 2092 Tunis, Tunisia*

[3]*Department of Physics, Yarmouk University, 21163 Irbid, Jordan*

[4]*Department of Applied Physics, Sharjah University, Sharjah, UAE*

(Received 22 May 2015; published 16 October 2015)

A thorough investigation of the effect of exchange and correlation on the electronic structure of wide-band-gap insulators ScF_3, YF_3, and AlF_3 is carried out using local, semilocal, and hybrid functionals in the density functional theory framework and the *GW* approximation with four current plasmon-pole models. It is shown that the hybrid functionals, which attribute more weight to electron exchange, lead to a decent agreement with the state of the art *GW* results, whereas the Tran-Blaha semilocal functional does not improve significantly the local density approximation results of the insulating transition-metal trifluorides, because of the high localization of the conduction band minimum states which are mainly of *d* character, and underestimate considerably the valence-band width of the studied materials.

DOI: 10.1103/PhysRevB.92.165202 PACS number(s): 71.15.Ap, 71.20.Nr, 71.15.Mb, 71.15.Nc

I. INTRODUCTION

During the last decade, the investigation of metal fluorides and rare-earth-doped metal fluorides has grown considerably due to their various applications in the technologies of glasses [1], batteries [2], optoelectronics [3], and also in hydrogen storage [4].

Several fluorides of trivalent metals MF_3 have ideal or distorted structures of the α-ReO_3 type, which are perovskite-like structures with the particularity of a vacancy occurring at the cation sites, hence a significant empty volume. This special property makes it possible to modify the physical properties by the insertion of crystal impurities, demonstrating the interest in this class of materials. Metal trifluorides are interesting materials for optical applications by dint of their transparency over a wide wavelength range. For example, glasses derived from ScF_3 are transparent from 0.3 μm in the ultraviolet region up to 7 μm in the infrared region [5]. Most MF_3 display a structural phase transition varying from 340 K in TiF_3 to 1250 K in CrF_3 [6] except ScF_3, which exhibits a negative thermal expansion and a stable cubic phase at ambient pressure and for a wide range of temperatures [7]. Thus at room temperature and at ambient pressure, scandium trifluoride adopts a cubic structure [see Fig. 1(a)], whereas all other metal trifluorides are either in a rhombohedral or orthorhombic structure [see Figs. 1(b) and 1(c)].

Few years ago, Greve *et al.* [8] discovered an astounding large and isotropic negative thermal expansion (NTE) for ScF_3, for a wide range of temperatures from 10 to about 1100 K, unlike ReO_3, which displays a low NTE below ambient temperature. Later, Li *et al.* [7] explained this property by the quartic potential giving rise to large amplitude transverse displacements of the fluorine atom, so that the two scandium atoms around it will be pulled together. It was noticed that the phase diagram of ScF_3 is very sensitive to structural defects and impurities, e.g., an applied hydrostatic pressure of about 0.15 GPa at 50 K gives rise to a phonon soft mode in the *M*-*R* high-symmetry direction of the Brillouin zone, leading to a transformation to rhombohedral $R\bar{3}c$ phase with two formula units per unit cell [9]. At ambient temperature, this phase transition was detected by x-ray diffraction and Raman spectroscopy under a hydrostatic pressure of 0.7 GPa and results from the rotation of the ScF_6 unit around the threefold axis. Under a pressure of 3.8 GPa, the rhombohedral structure transforms further into an orthorhombic *Pnma* structure with four formula units per unit cell and the Raman spectrum shows the existence of two soft phonon modes [9]. Lanthanide-ion-doped ScF_3 nanocrystals exhibit multicolor ultraviolet, photoluminescence, cathode luminescence, and up-conversion luminescence, as well as ferromagnetic properties [10]. Extensive efforts were made to control the thermal expansion of ScF_3 within solid solution formation by adding Y, Al, and Ti ions [11–13].

At room temperature, the yttrium trifluoride exhibits the β-YF_3 structure, as orthorhombic *Pnma* with four formula units per unit cell, where the fluorine atoms occupy the 4c and 8d Wyckoff sites [see Fig. 1(c)]. YF_3 doped by rare earth ions can be a good candidate to produce efficient visible emission under vacuum ultraviolet (UV) irradiation and consequently, it can be efficient in transforming vacuum UV light into visible one [14]. Using time resolved emission and excited spectra [15], two intrinsic luminescence bands peaking at 4.5 and 5.6 eV due to the radiative recombination of self-trapped exciton were observed, suggesting that YF_3 can be used as a wavelength selective optical filter in the 157-nm photolithography instead of the CaF_2 crystal, since YF_3 can be grown at lower temperature than CaF_2 [16] and when doped, YF_3 crystals can be used as a refractive medium in the vacuum UV region.

The YF_3 compound was studied by angular dispersive synchrotron x-ray diffraction [17] and it transforms to a hexagonal $P\bar{3}c1$ structure with six formula units per unit cell at a hydrostatic pressure of 7.5 GPa. Due to its wide band gap and suitable Y^{3+} sites without additional charge compensation [15], YF_3 can also be used as a solid-state laser or a scintillator, since it can be easily doped with rare-earth ions.

However, AlF_3 adopts the α-AlF_3 rhombohedral structure at ambient conditions [18] [see Fig. 1(b)] and exhibits a

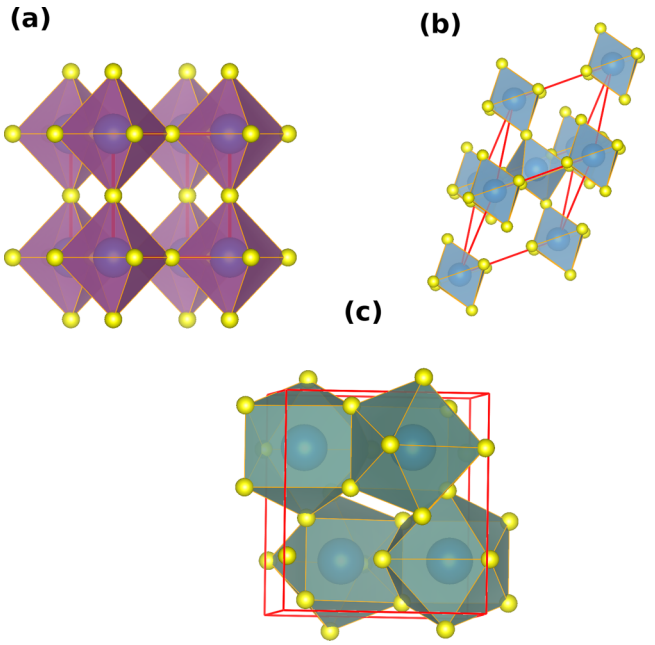

FIG. 1. (Color online) Crystal structure of MF_3: (a) shows the α-ReO_3 cubic phase of ScF_3, the scandium atom (in blue) occupy the center of ScF_6 octahedron and the fluorine atoms are located at the corners (in yellow), (b) the rhombohedral $R\bar{3}c$ phase of AlF_3 with two formula units per unit cell, and (c) the *Pnma* orthorhombic phase of YF_3 with four formula units per unit cell.

phase transition to a cubic structure at 730 K [6,19,20]. This transformation was confirmed by molecular dynamics simulations [21] and pair distribution function analysis [22] and the cubic phase was revealed to contain local octahedral tilts. When heated, the bond angle connecting one fluorine atom and two aluminum atom neighbors increases steadily with temperature up to 1100 K. Furthermore, the distance separating one aluminum and one fluorine atom does not vary significantly with temperature, which indicates the rigidity of the AlF_6 octahedra [22]. Chen and coworkers also did an interesting calculation, where their local density approximation $T = 0$ K energy surface in the structural parameter space shows that the minimum corresponds to the observed rhombohedral structure [23]. However, their calculated band gap is too small compared to experiment.

As the electronic structure of a material is a basic ingredient for understanding its physical properties, we begin by an investigation of that of ScF_3, stressing the effect of different approximations to the exchange correlation functional on its insulating energy band gap. In particular, we show that the Tran-Blaha [24] functional, which worked nicely for *sp* semiconductors and insulators fails for materials such as ScF_3 due to the presence of Sc *d* electrons. To show which hybrid functional provides the best band gaps for wide gap insulators containing *d* electrons, we extend this study by performing various flavors of plasmon-pole *GW* calculations, where *G* is the Green's function and *W* the screened Coulomb interaction. To confirm our findings, we also extended this study to YF_3 with $4d^1$ electrons and AlF_3 without *d* electrons. To the best of our knowledge, the hybrid functionals and *GW* ground-state electronic properties of scandium trifluoride and aluminum trifluoride are not yet computed. The only calculations available in the literature concern the electronic structure of AlF_3 (Ref. [23]) and YF_3 (Ref. [25]) and are based on LDA. In both calculations, the insulating band gaps are much smaller than the experimental values. Our calculations will therefore improve upon these LDA results.

This paper is organized as follows. In Sec. II, we introduce explicitly our theoretical framework, focusing on the various density functional theory (DFT) exchange and correlation hybrid functionals and the four different plasmon-pole model *GW* approximations used in this work. In Sec. III, we explore in details, in the spirit of the mentioned hybrid functionals, the effect of different exchange-correlation approximations on the electronic structure of ScF_3 and the physical properties obtained form the band structure, like the density of states, the energy band gap, the effective masses and the equation of state (pressure-volume relation). This study is then extended to the electronic structure of YF_3 and AlF_3.

II. THEORETICAL BACKGROUND

A. Semilocal functionals

The state of the art DFT [26,27] provides an efficient *ab initio* method for accurate studies of the ground-state properties of various materials. In this work, we concentrate on the effect of DFT exchange-correlation functionals on the electronic structure of ScF_3 and related wide-band-gap materials. We propose to find the best functional for accurately describing the electron-electron interaction leading to an accurate description of its electronic structure. To this end, we propose first to use a metageneralized gradient correction (Meta-GGA) exchange potential combined with the local density approximation (LDA) correlation proposed by Tran and Blaha [24], which has already successfully predicted band gaps for a large variety of semiconductors and insulators, in close agreement with experiment. This Tran-Blaha potential is given by

$$v_x(\mathbf{r}) = c_{\mathrm{TB09}} v_x^{\mathrm{BR89}}(\mathbf{r}) + (3c_{\mathrm{TB09}} - 2)\sqrt{\frac{5t(\mathbf{r})}{6\pi^2\rho(\mathbf{r})}}, \quad (1)$$

where t is the kinetic energy density, ρ the electronic density, and v_x^{BR89} an approximation of the Coulomb hole exchange potential introduced by Becke-Roussel [28]:

$$v_x^{\mathrm{BR89}}(\mathbf{r}) = -\frac{1 - e^{-x(\mathbf{r})} - \frac{1}{2}x(\mathbf{r})e^{-x(\mathbf{r})}}{\left(\frac{x^3(\mathbf{r})e^{-x(\mathbf{r})}}{8\pi\rho(\mathbf{r})}\right)^{\frac{1}{3}}}. \quad (2)$$

The $x(\mathbf{r})$ function satisfies the relation

$$\frac{x(\mathbf{r})e^{-\frac{2}{3}x(\mathbf{r})}}{(x(\mathbf{r}) - 2)} = \frac{2}{3}\pi^{\frac{2}{3}}\frac{\rho^{\frac{5}{3}}(\mathbf{r})}{\frac{1}{6}\left[\nabla^2\rho(\mathbf{r}) - \frac{8}{5}\left(t(\mathbf{r}) - \frac{1}{4}\frac{\nabla^2\rho(\mathbf{r})}{\rho(\mathbf{r})}\right)\right]}. \quad (3)$$

The Tran-Blaha implicit variable of the system is given by

$$c_{\mathrm{TB09}} = \alpha + \beta\left(\frac{1}{\Omega}\int_{\Omega}\frac{|\nabla\rho(\mathbf{r}')|}{\rho(\mathbf{r}')}d^3r'\right)^{\frac{1}{2}} \quad (4)$$

where Ω is the unit cell volume and α, β are two adjustable parameters. The default values obtained from a fit of many semiconductors [24] are $\alpha = -0.012$ and $\beta = 1.023\ \text{bohr}^{\frac{1}{2}}$.

B. Hybrid functionals

One of the deficiencies of the semilocal density approximations is the neglect of self-interaction correction, which leads to an artificial delocalization of the wave functions resulting in an underestimation of electron excitation energies, and hence of the band gap value. On the contrary, hybrid exchange-correlation functionals [29] do not suffer much from self-interaction effects, leading to a great improvement in the predicted electronic properties. The main feature of hybrid functionals is that the exchange correlation potential has an explicit orbital dependence, which is not the case for semilocal functionals. For hybrid functionals, the width of the band gap of materials increases linearly with the amount of the exact exchange:

$$E_{\text{xc}}^{\text{hyb}} = \alpha_1 E_x^{\text{HF}} + \alpha_2 E_x^{\text{slF}} + \alpha_3 E_c^{\text{slF}}, \tag{5}$$

where E_x^{HF} is the nonlocal Hartree-Fock exchange energy, constructed using Kohn-Sham orbitals, and $E_{x(c)}^{\text{slF}}$ is the exchange (correlation) energy obtained from semilocal functionals (slF). The parameters $\alpha_p\{p = 1,2,\text{or } 3\}$ control, respectively, the contribution of E_x^{HF}, E_x^{slF} and E_c^{slF},

$$E_x^{\text{HF}}(\mathbf{r},\mathbf{r}') = -\frac{1}{2}\sum_{i,j}\int d^3r d^3r' \frac{\varphi_i^\star(\mathbf{r})\varphi_j(\mathbf{r})\varphi_j^\star(\mathbf{r}')\varphi_i(\mathbf{r}')}{|\mathbf{r}-\mathbf{r}'|}. \tag{6}$$

In this paper, we employ three hybrid functionals: B3LYP [30], PBE0 [31], and HSE06 [32] and compare their effect on the electronic structure of wide-band-gap ScF_3 and related compounds. Likewise, we compare the results of these functionals to those obtained by means of various plasmon-pole GW calculations. The first hybrid functional depends on three parameters, hence called B3LYP and is given by

$$\begin{aligned} E_{\text{xc}}^{\text{B3LYP}} = {} & E_x^{\text{LDA}} + \alpha_1\left(E_x^{\text{HF}} - E_x^{\text{LDA}}\right) + \alpha_2\left(E_x^{\text{GGA}} - E_x^{\text{LDA}}\right) \\ & + \alpha_3\left(E_c^{\text{GGA}} - E_c^{\text{LDA}}\right), \end{aligned} \tag{7}$$

where the mixture between Hartree-Fock exchange and semilocal exchange is governed respectively by the parameters $\alpha_1 = 0.2$ and $\alpha_2 = 0.72$, and the correlation part by $\alpha_3 = 0.81$.

The exchange-correlation energy corresponding to the hybrid functional PBE0 is given by

$$E_{\text{xc}}^{\text{PBE0}} = \tfrac{1}{4}E_x^{\text{HF}} + \tfrac{3}{4}E_x^{\text{PBE}} + E_c^{\text{PBE}}. \tag{8}$$

Usually, this hybrid functional overestimates the band gaps of small band gap materials and underestimates those of large band gap ones [33].

In the HSE06 hybrid functional, the electron-electron exchange interaction is partitioned into short-range (SR) and long-range (LR) parts. The exchange-correlation energy is then given by

$$\begin{aligned} E_{\text{xc}}^{\text{HSE06}} = {} & \alpha E_x^{\text{HF,SR}}(\mu) + (1-\alpha)E_x^{\text{PBE,SR}}(\mu) \\ & + \alpha E_x^{\text{PBE,LR}}(\mu) + E_c^{\text{PBE}}. \end{aligned} \tag{9}$$

This energy can be seen as an approximated contribution to the self-energy in the GW approximation, whose Coulomb interaction is screened by the mixing parameter α instead of the inverse of dynamical dielectric matrix in the many-body perturbation theory (MBPT). The parameter μ controls the range separation, i.e., its inverse represents the critical distance at which the short-range Coulomb interaction can be assumed to be negligible. This decomposition can be obtained through the error function erf:

$$\frac{1}{r} = \frac{(1-\text{erf}(\mu r))}{r} + \frac{\text{erf}(\mu r)}{r}, \tag{10}$$

where the first term represents the short-range contribution that is treated with a Fock operator, whereas the second one corresponds to the long-range contributions and is treated using semilocal exchange functionals.

Taking $\alpha = 0$ in the expression of the HSE06 energy reduces it to the PBE energy, while in the case of $\mu = 0$, it turns it to PBE0 energy. The short-range contributions to Hartree-Fock exchange energy can be written as

$$\begin{aligned} E_x^{\text{HF,SR}}(\mathbf{r},\mathbf{r}') = {} & -\frac{1}{2}\sum_{i,j}\int d^3r d^3r'(1-\text{erf}(\mu|\mathbf{r}-\mathbf{r}'|)) \\ & \times \frac{\varphi_i^\star(\mathbf{r})\varphi_j(\mathbf{r})\varphi_j^\star(\mathbf{r}')\varphi_i(\mathbf{r}')}{|\mathbf{r}-\mathbf{r}'|}. \end{aligned} \tag{11}$$

Writing the effective static dielectric constant ε_∞ as the inverse of α gives an effective screening matrix corresponding to HSE06 following this expression [34,35]:

$$W^{\text{HSE06}}(\mathbf{r},\mathbf{r}') = \alpha\frac{(1-\text{erf}(1-\mu|\mathbf{r}-\mathbf{r}'|))}{|\mathbf{r}-\mathbf{r}'|}. \tag{12}$$

The band gap increases almost linearly with increasing α and is inversely proportional to μ [36].

C. GW approximation

The treatment of properties related to neutral excitation processes, like band structures and Fermi surfaces, where an electron is excited from the valence to the unoccupied conduction bands in direct photoemission spectroscopy, via an impinging photon, can be achieved by the so-called one-particle Green function or propagator in the framework of MBPT. The variation of the electron density due to these excitations is well described by the polarizability χ.

In the DFT formalism, the interactions in the system are described by the Kohn-Sham equations for each state n:

$$\begin{aligned} & \left[-\frac{\nabla^2}{2} + \int d^3r'\rho(\mathbf{r}')v_{ext}(\mathbf{r}') + \int d^3r'\rho(\mathbf{r}')v(\mathbf{r}-\mathbf{r}')\right. \\ & \left. + v_{\text{xc}}[\rho](\mathbf{r})\right]\varphi_n^{\text{KS}}(\mathbf{r}) = \epsilon_n^{\text{KS}}\varphi_n^{\text{KS}}(\mathbf{r}), \end{aligned} \tag{13}$$

whereas, in the MBPT, the corresponding equations describing quasiparticles are given by

$$\begin{aligned} & \left[-\frac{\nabla^2}{2} + \int d^3r'\rho(\mathbf{r}')v_{\text{ext}}(\mathbf{r}') + \int d^3r'\rho(\mathbf{r}')v(\mathbf{r}-\mathbf{r}')\right]\varphi_n^{\text{QP}}(\mathbf{r}) \\ & + \int d^3r'\Sigma\left(\mathbf{r},\mathbf{r}';\epsilon_n^{\text{QP}}\right)\varphi_n^{\text{QP}}(\mathbf{r}') = \epsilon_n^{\text{QP}}\varphi_n^{\text{QP}}(\mathbf{r}), \end{aligned} \tag{14}$$

where Σ represents the electronic self-energy and contains all the many-body exchange and correlation effects beyond the

usual Hartree potential. The determination of its expression relies on the resolution of the set of Hedin equations [37]. The neglect of vertex corrections gives the so-called GW approximation, where G is the one-electron Green function and W the screened Coulomb interaction. The self-energy is then written as a convolution product of the one-electron Green's function G and the dynamically screened Coulomb interaction W:

$$\Sigma(\mathbf{r},\mathbf{r}';\omega) = \frac{i}{2\pi}\int d\omega' e^{i\eta\omega'} G(\mathbf{r},\mathbf{r}';\omega+\omega')W(\mathbf{r}',\mathbf{r};\omega'), \tag{15}$$

where the screening by the inverse dielectric matrix is calculated in the random phase approximation in reciprocal space:

$$W_{\mathbf{G}\mathbf{G}'}(\mathbf{q},\omega) = \frac{4\pi}{|\mathbf{q}+\mathbf{G}|^2}\epsilon^{-1}_{\mathbf{G}\mathbf{G}'}(\mathbf{q},\omega). \tag{16}$$

The dielectric matrix is given by

$$\epsilon(\mathbf{r},\mathbf{r}';\omega) = \frac{1}{\Omega}\sum_{\mathbf{q},\mathbf{G},\mathbf{G}'} e^{i(\mathbf{q}+\mathbf{G})\cdot\mathbf{r}}\epsilon_{\mathbf{G}\mathbf{G}'}(\mathbf{q},\omega)e^{-i(\mathbf{q}+\mathbf{G}')\cdot\mathbf{r}'}. \tag{17}$$

The quasiparticle energies and lifetimes obtained from the GW approximation can be directly compared to the ones measured by direct or inverse photoemission.

The inhomogeneous density matrix distribution is described by the off-diagonal elements of the dielectric matrix $\epsilon(\mathbf{G}\neq\mathbf{G}')$. The self-energy can be decomposed into exchange and correlation terms, where the exchange term is given by

$$\langle\varphi_{\mathbf{k},b}|\Sigma_x|\varphi_{\mathbf{k},b}\rangle = -\frac{4\pi}{\Omega}\sum_{\mathbf{q}}\sum_{b'}^{occ}\sum_{\mathbf{G}}\frac{\left|M^{b,b'}_{\mathbf{G}}(\mathbf{k},\mathbf{q})\right|^2}{|\mathbf{q}+\mathbf{G}|^2}, \tag{18}$$

and where $M^{b,b'}_{\mathbf{G}}$ represents the so-called oscillator strength. Here, b and b' denote the band index. The correlation self-energy term is given by

$$\langle\varphi_{\mathbf{k},b}|\Sigma_c|\varphi_{\mathbf{k},b}\rangle = \frac{1}{\Omega}\sum_{\mathbf{q}}\sum_{\mathbf{G}\mathbf{G}'}\sum_{b'}\left[M^{b,b'}_{\mathbf{G}}(\mathbf{k},\mathbf{q})\right]^{\star} \times M^{b,b'}_{\mathbf{G}'}(\mathbf{k},\mathbf{q})I_{\mathbf{G}\mathbf{G}'}(\mathbf{k},\mathbf{q},\omega), \tag{19}$$

where $I_{\mathbf{G}\mathbf{G}'}$ is expressed as

$$I_{\mathbf{G}\mathbf{G}'}(\mathbf{q},\mathbf{k},\omega) = \frac{i}{2\pi}\int d\omega' \frac{W_p(q,\omega')}{\omega+\omega'-\epsilon_b(\mathbf{k}-\mathbf{q})+i\delta\ \mathrm{sgn}[\epsilon_b(\mathbf{k}-\mathbf{q})-\mu]}. \tag{20}$$

Here, μ denotes the Fermi level and W_p the difference between the dynamical screened potential W and the bare potential v.

The screened W is anticipated to be smaller than v and gives a more accurate description of the electron-electron interactions in mean-field approximations such as LDA, GGA, Meta-GGA (TB09) of independent particles in the DFT framework.

The correlation part of the self-energy $\Sigma_c = iGW_p$ is non-Hermitian and gives access to the finite lifetimes of quasiparticles and satellite structures in the spectral functions. Considering the similarities between the two equations (13) and (14) and the assumption that the Kohn-Sham and quasiparticle wave functions are very similar [38], a perturbative approach is therefore reasonable. So the first-order perturbative approach for each state n leads to

$$\epsilon^{GW}_n = \epsilon^{\mathrm{KS}}_n + \mathcal{Z}_n\langle\varphi^{\mathrm{KS}}_n|\Sigma\left(\epsilon^{\mathrm{KS}}_n\right) - V_{\mathrm{xc}}|\varphi^{\mathrm{KS}}_n\rangle, \tag{21}$$

where the renormalization factor $\mathcal{Z}$ is given by

$$\mathcal{Z}_n = \left(1 - \left\langle\varphi^{\mathrm{KS}}_n\left|\frac{\partial\Sigma(\omega)}{\partial\omega}\right|_{\epsilon^{\mathrm{KS}}_n}\right|\varphi^{\mathrm{KS}}_n\right\rangle\right)^{-1}. \tag{22}$$

A full study of the frequency dynamical effects of the screened interaction in reciprocal space is numerically cumbersome, so the problem of the dependence on the frequencies ω of both the dielectric matrix and the self-energy is handled in this work by various plasmon-pole models. From these approximations, we can easily make an analytic study of the convolution of the Green's functions and the Coulomb screening potential in frequency space. Unless explicitly stated, most GW calculations conducted in this work are non-self-consistent and use LDA as a starting point. It is well documented in the literature that the ensuing quasiparticle energies depend on the starting point used to calculate the input single-particle energies and wave functions [39–41], however, it has also been shown that it accurately predicts the band gaps of most semiconductors with high accuracy [42]. Usually, in the literature this approximation is called G_0W_0 but here since there is no confusion we call it GW.

In the following, we focus on the current four plasmon-pole models in the description of the electronic interactions: the Godby-Needs [43] (GN), the Hybersten and Louie [38] (HL), the von der Linden and Horsch [44] (VLH), and the Engel-Farid [45] (EF) models.

The GN plasmon-pole model gives an easy evaluation of the dynamical behavior of the screened interaction and the convolution integral of the correlation part of the self-energy, only by taking the static frequency limit and one imaginary frequency, which can be considered as the effective frequency of the plasmon excitation. The imaginary part of the inverse dielectric matrix is written as

$$\mathrm{Im}\left\{\epsilon^{-1}_{\mathbf{G}\mathbf{G}'}(\mathbf{q},\omega)\right\} = A_{\mathbf{G}\mathbf{G}'}(\mathbf{q})[\delta(\omega-\widetilde{\omega}_{\mathbf{G}\mathbf{G}'}(\mathbf{q})) - \delta(\omega+\widetilde{\omega}_{\mathbf{G}\mathbf{G}'}(\mathbf{q}))], \tag{23}$$

where A is the weight of the peak of the imaginary response function $\epsilon_{\mathbf{G}\mathbf{G}'}(\mathbf{q},\omega)$ with respect to ω in both diagonal and off-diagonal elements. The real part is given by

$$\mathrm{Re}\left[\epsilon^{-1}_{\mathbf{G}\mathbf{G}'}(\mathbf{q},\omega)\right] = \delta_{\mathbf{G}\mathbf{G}'} + \frac{\Omega^2_{\mathbf{G}\mathbf{G}'}(\mathbf{q})}{\omega^2-\widetilde{\omega}^2_{\mathbf{G}\mathbf{G}'}(\mathbf{q})}, \tag{24}$$

where $\widetilde{\omega}$ defines the pole frequency and $\Omega_{\mathbf{G}\mathbf{G}'}$ the effective bare plasma frequency.

In the HL plasmon-pole model, the dynamical effects are included through the calculation of dielectric function only in the static limit, and then extended to finite frequencies

by means of the f-sum rule. The A and $\widetilde{\omega}$ parameters are determined from the Kramers-Kronig relations and the generalized version of the Johnson f-sum rules:

$$\Omega^2_{\mathbf{G}\mathbf{G}'}(\mathbf{q}) = \omega^2_{pl}\frac{(\mathbf{q}+\mathbf{G})\cdot(\mathbf{q}+\mathbf{G}')}{|\mathbf{q}+\mathbf{G}|^2}\frac{\rho(\mathbf{G}-\mathbf{G}')}{\rho(0)}, \tag{25}$$

$$\widetilde{\omega}_{\mathbf{G}\mathbf{G}'}(\mathbf{q}) = \frac{\Omega^2_{\mathbf{G}\mathbf{G}'}(\mathbf{q})}{\delta_{\mathbf{G}\mathbf{G}'} - \epsilon^{-1}_{\mathbf{G}\mathbf{G}'}(\mathbf{q},\omega=0)}, \tag{26}$$

$$A_{\mathbf{G}\mathbf{G}'}(\mathbf{q}) = -\frac{\pi}{2}\frac{\Omega_{\mathbf{G}\mathbf{G}'}(\mathbf{q})}{\widetilde{\omega}_{\mathbf{G}\mathbf{G}'}(\mathbf{q})}, \tag{27}$$

where $\rho(\mathbf{G}-\mathbf{G}')$ is the electron density in reciprocal space.

The VLH plasmon-pole model relies on the assumption that only the eigenvalues of the Hermitian dielectric matrix $\widetilde{\epsilon}$ contain the frequency dependence, which can be written as

$$\widetilde{\epsilon}_{\mathbf{G}\mathbf{G}'}(\mathbf{q},\omega) = \frac{|\mathbf{q}+\mathbf{G}|}{|\mathbf{q}+\mathbf{G}'|}\epsilon_{\mathbf{G}\mathbf{G}'}(\mathbf{q},\omega), \tag{28}$$

where the eigenvalues are given by

$$\lambda^{-1}_{n,\mathbf{q}}(\omega) = 1 + \frac{\left(1-\lambda^{-1}_{n,\mathbf{q}}(0)\right)}{2}\omega_n(\mathbf{q}) \times\left[\frac{1}{\omega-\omega_n(\mathbf{q})-i\delta} - \frac{1}{\omega+\omega_n(\mathbf{q})-i\delta}\right]. \tag{29}$$

Here, n numbers the eigenvalues of the Hermitian dielectric matrix, and the plasmon-pole frequencies follow also the f-sum rule:

$$\omega^2_n(\mathbf{q}) = \frac{\omega^2_{pl}}{\left(1-\lambda^{-1}_{n,\mathbf{q}}(0)\right)}\sum_{\mathbf{G}\mathbf{G}'}\frac{(\mathbf{q}+\mathbf{G})\cdot(\mathbf{q}+\mathbf{G}')}{|\mathbf{q}+\mathbf{G}||\mathbf{q}+\mathbf{G}'|} \times X^{\star}_{n,\mathbf{q}}(\mathbf{G})\frac{\rho(\mathbf{G}-\mathbf{G}')}{\rho(0)}X_{n,\mathbf{q}}(\mathbf{G}'). \tag{30}$$

Here, $X_{n,\mathbf{q}}$ are the matrix elements established by the eigenvectors of the inverse dielectric matrix. Accordingly, the plasmon frequencies obtained from this model are all real and the treatment of the off-diagonal elements for the dielectric matrix is improved, contrary to the previous approach suggested by Hybersten and Louie.

In the EF plasmon-pole model, both the eigenvalues and eigenvectors depend on frequency. The EF model approximates the full polarizability χ by another $\widetilde{\chi}$, which are similar in the static and high frequency limits:

$$\widetilde{\chi}^{-1}_{\mathbf{G},\mathbf{G}'}(\mathbf{q},\omega) = \sum_n Y_{n,\mathbf{q}}(\mathbf{G})\left(\omega^2-\omega^2_n(\mathbf{q})\right)Y^{\star}_{n,\mathbf{q}}(\mathbf{G}'). \tag{31}$$

The $Y_{n,\mathbf{q}}$ are the eigenvectors of the full polarizability χ. Consequently, in this plasmon-pole model, we can interpret the eigenenergies as plasmon energies and their small $\mathbf{q}$ expansion gives the plasmon dispersion coefficients.

D. Computational details

Most of our DFT and GW calculations were carried out using the ABINIT package [46] with a plane-wave basis set, whereas the quasiparticle band structure is obtained from the Wannier interpolation [47]. To calculate the electronic structures in the framework of hybrid functionals, we employed the QUANTUM ESPRESSO package [48]. The interactions between valence electrons and ionic cores is described by the norm-conserving pseudopotentials generated according to the Troullier-Martins scheme [49] with the APE package [50]. Both the semicore electrons $3s^2\ 3p^6$ of the $3d$ transition-metal Sc and the $4s^2\ 4p^6$ of Y are treated as valence electrons. The inclusion of these semicore states is important for determining accurately the energy band gaps of these materials.

The number of plane waves are selected using a kinetic energy cutoff of 100 Ry for the three studied materials, which are found to give well converged structural and electronic properties. Brillouin zone integrations are made using a Γ-centered $\mathbf{k}$-point mesh sampling of $12\times12\times12$ Monkhorst-Pack grid [51] for ScF_3 and AlF_3, and for YF_3 a Γ-centered $\mathbf{k}$-point mesh sampling of $12\times12\times16$ was employed.

The divergence in the derivative of the orbital energies, when handling the Fock operator with respect to small $\mathbf{q}$ vectors, is treated with the Gygi Baldereschi approach [52]. A $\mathbf{q}$-point mesh sampling of $4\times4\times4$ for the Fock operator was employed in the hybrid functionals calculation in the case of ScF_3 and AlF_3, while a $3\times3\times4\mathbf{q}$-point mesh has been used in the case of YF_3. The problem of the integrable singularities is treated following the Spencer-Alavi method [53], which makes a simple modification to the Coulomb potential in the exchange self-energy integral, and then the singularity is removed without the inclusion of any auxiliary function. The size of the dielectric matrix used was determined by a kinetic energy cutoff of 70 Ry. The main stalemate in the accuracy of a GW calculation is the requirement of a summation over a huge number of empty states to represent efficiently the Hilbert space. We used the extrapolar approximation proposed by Bruneval *et al.* [54], which replaces the effects of the empty states beyond a certain limit by an adjustable energy.

III. RESULTS AND DISCUSSION

Scandium trifluoride has the space group $Pm\bar{3}m$ number 221 [see Fig. 1(a)]. The experimental lattice parameter is used in all calculations and is equal to 4.01 Å, taken from Aleksandrov *et al.* [55].

In order to get the electronic structure, we first used the LDA. For the calculated density of states, we employed the tetrahedron method [56]. ScF_3 was found to have a direct band gap of 6.78 eV and an indirect band gap of 6.25 eV. The bottom of the conduction band is located at the Γ high-symmetry point and the top of the valence band at the R point (see Fig. 7). This wide band gap rules out the possibility that electronic excitations can play a role in the negative thermal expansion. From the analysis of the partial density of states (Fig. 2), it appears that the $2p$ fluorine states are mainly responsible for the character of the upper valence bands, while the lowest conduction bands originate mostly from the $3d$ states of the scandium ion. The results seem therefore to agree with the formal ionic model of Sc^{3+} as determined from photoemission [57,58]. This is due to the strong electronegativity of the fluorine atom and the strong Sc $3d$ and F $2p$ hybridization. However, the LDA bandwidth is about 3.2 eV, which is a bit short of the experimental value [58] of 4 eV (full width at half maximum). We show later, that the GW calculation improves

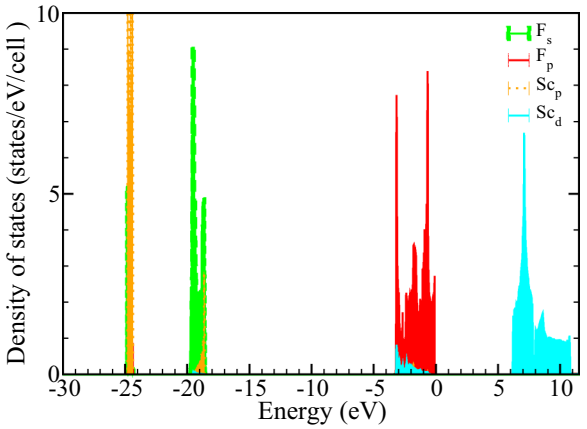

FIG. 2. (Color online) LDA calculated partial density of states of ScF_3: the $2p$ fluorine states (hatched red) are the main responsible of the valence-band maximum (VBM). The conduction-band minimum (CBM) originates from the $3d$ states of the scandium atom (filled cyan). The top of valence states is at zero energy.

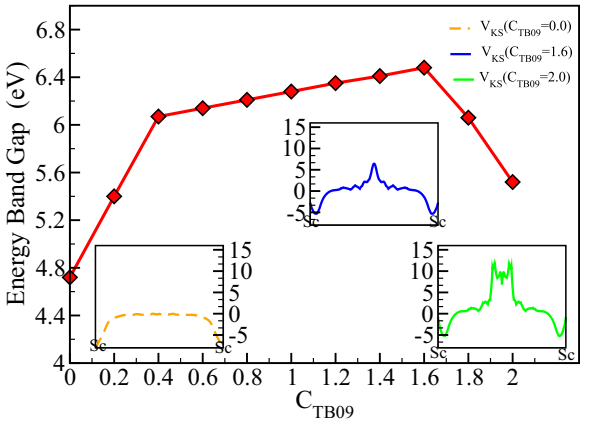

FIG. 3. (Color online) Change of the band gap as a function of the value of the c_{TB09} parameter. (Inset) Kohn-Sham potential along [111] direction is presented for three special cases, i.e., for the lowest band gap (orange), the highest band gap (blue), and within an intermediate band gap (green).

only slightly the bandwidth, whereas the TB09 functional will worsen it by about 1 eV. The p states of scandium are responsible for the deeper bands at around -25 eV, whereas the contribution of the s states of fluorine appears in the range of -19 eV. The photoemission data [57,58] show that those states are located at -28 and -24 eV, respectively. Here, also we show that GW improves the results by only 1 eV compared to experiment.

A volume cell optimization for ScF_3 was carried out in the framework of local, semilocal PBE, and hybrid functionals PBE0. We found that LDA slightly underestimates the experimental lattice parameter (3.99 Å) and gives a bulk modulus equal to 74.1 GPa, which is comparable to the value of 70.2 GPa obtained from Raman spectroscopy [9], whereas the PBE and PBE0 functionals overestimate the experimental lattice constant and give respectively 4.07 and 4.04 Å. The PBE gives a bulk modulus of 60.5 GPa whereas PBE0 gives 57.5 GPa, in good agreement with the 57 GPa value obtained from x-ray spectroscopy [8]. This latter agreement is certainly fortuitous since this functional overestimates the lattice parameter.

The high hybridization between scandium d bands and p fluoride bands is not well described within the LDA, which is reflected in an underestimation of the band gap. The band gap of ScF_3 is therefore calculated within the metageneralized gradient approximation of Tran-Blaha. This functional produced just a small enhancement of about 0.3 eV compared to the LDA value. A surprising correction since this functional is supposed to give the correct gaps in close agreement with experiment for many sp semiconductors. One way to adjust the Tran-Blaha functional is to use c_{TB09} as a free parameter instead of using the expression given in Eq. (4) to study its effect on the size of the band gap. We made calculations for c_{TB09} in the range of [0,2]. As shown in Fig. 3, an increase of the band gap is observed with respect to the size exchange amount, until the value of c_{TB09} reaches the value obtained self-consistently. Beyond this value the band gap decreases steadily.

The Kohn-Sham potential of ScF_3 is presented in Fig. 3 along the [111] direction linking two scandium atoms and passing through the empty volume of the cube. It presents a positive peak in the center of the volume for c_{TB09} equal to 1.6 or 2.0, whereas there is no peak in the case of $c_{\mathrm{TB09}} = 0.0$. The peak found in $c_{\mathrm{TB09}} = 2.0$ is similar to the one for the cases where c_{TB09} is different from 0.0 and 1.6, with a small difference in the peak amplitude. In previous studies [59,60], an adjustment of the parameter c_{TB09} led to an agreement with the experimental band gap, so increasing the c_{TB09} value resulted in an increase of the band gap. It is not exactly the case for ScF_3. The parameter c_{TB09} obtained from our self-consistent calculation for scandium trifluoride is equal to 1.6, in good agreement with Tran-Blaha predictions [24] for wide-band-gap systems, i.e, in the range of 1.4–1.7, whereas for low-band-gap semiconductors, the predicted value for c_{TB09} is between 1.1 and 1.3. To get more insight into the failure of TB09 functional to describe properly the band gap of ScF_3, we investigated separately the correction of this functional to the conduction-band minimum (CBM) and the valence-band maximum (VBM). We considered TB09 as a first-order perturbation to LDA eigenvalues:

$$\epsilon_n^{\mathrm{TB09}} = \epsilon_n^{\mathrm{LDA}} + \int \rho_n^{\mathrm{LDA}}(\mathbf{r})\big[V_{KS}^{\mathrm{TB09}}(\mathbf{r}) - V_{\mathrm{KS}}^{\mathrm{LDA}}(\mathbf{r})\big]d^3r, \quad (32)$$

where $\rho_n^{\mathrm{LDA}}(\mathbf{r}) = |\Psi_n^{\mathrm{LDA}}(\mathbf{r})|^2$ is the electron density of the state n. The band-gap correction of TB09 to LDA is therefore given by

$$\Delta\varepsilon_g = \int \big[\rho_{CBM}^{\mathrm{LDA}}(\mathbf{r}) - \rho_{VBM}^{\mathrm{LDA}}(\mathbf{r})\big]\big[V_{\mathrm{KS}}^{\mathrm{TB09}}(\mathbf{r}) - V_{\mathrm{KS}}^{\mathrm{LDA}}(\mathbf{r})\big]d^3r$$
$$= \Delta\varepsilon^{\mathrm{CBM}} - \Delta\varepsilon^{\mathrm{VBM}}. \quad (33)$$

Table I shows the shifts of the top of the valence bands and the bottom of the conduction bands, the LDA and TB09

TABLE I. LDA and TB09 band gaps E_g compared to experiment (for ScF_3 in absence of the experimental value, we used our calculated GW result within the GN plasmon-pole model) and TB09 correction to the LDA for the VBM ($\Delta\varepsilon^{\mathrm{VBM}}$) and the CBM ($\Delta\varepsilon^{\mathrm{CBM}}$). The TB09 corrections as a first-order perturbation to LDA are between parentheses. All values are in eV.

Material	E_g (LDA)	E_g (TB09)	$\Delta\varepsilon^{\mathrm{VBM}}$	$\Delta\varepsilon^{\mathrm{CBM}}$	E_g(Expt.)
ScN	−0.11	0.75	0.11 (0.31)	0.97 (1.04)	1.3 ± 0.3,[a] 1.4 ± 0.2[a] 0.9 ± 0.1 eV[a]
Si	0.46	0.93	−0.59 (−0.58)	−0.12(−0.10)	1.17[b]
ScF_3	6.25	6.57	2.63(3.91)	2.95(3.92)	11.16[c]
LiF	8.79	14.34	1.60(1.68)	7.15(6.72)	14.2[d]
CaF_2	6.74	12.9	1.86 (1.94)	8.02(8.05)	11.8[e]
AlF_3	7.23	13.06	1.95(1.23)	7.78(8.57)	10.8[f]
YF_3	7.53	9.04	1.28(1.47)	2.79(3.12)	12.5[g]

[a]References [61,62,68].
[b]Reference [63].
[c]Our GW value.
[d]Reference [64].
[e]Reference [65].
[f]Reference [66].
[g]Reference [15].

band gaps, as well as the experimental band gaps (in absence of experimental gaps, our GW gaps are taken as reference for ScF_3). The smallest change in this comparative study corresponds to ScF_3, which has a comparable correction to the conduction and valence bands. Consequently, the two shifts cancel each other and the resulting correction to the band gap is negligible compared to other studied materials. The first-order perturbation correction can be very close to the exact values, whose correction could be larger than half the gap value in the case of ScN and CaF_2.

Figure 4 presents the integrand of Eq. (32) to the calculated $\Delta\varepsilon_g$ as given in Eq. (33) for ScF_3 in the (100) plane and AlF_3 in the (110) plane. It is clear that the integral of the integrand for the VBM and CBM will cancel each other for ScF_3 but not for AlF_3. This is due to the fact that the CBM of ScF_3 is mostly of e_g symmetry and is very localized on the Sc atom (see Fig. 7) whereas for AlF_3 it is very extended and shared by both Al and fluorine (see Fig. 9). The situation is also similar for YF_3 (see Fig. 10).

Despite the use of the semilocal approximation to the exchange interaction, which resulted in more localized electrons, TB09 does not show a significant enhancement to the band gap compared to LDA. One reason of this small correction is the fact that the Tran-Blaha functional failed to describe strongly correlated d or f states [67]. As indicated in Table I and Fig. 4, the corrections $\Delta\varepsilon^{\mathrm{CBM}}$ and $\Delta\varepsilon^{\mathrm{VBM}}$ are very similar in the case of ScF_3, which lead to a very small gap correction $\Delta\varepsilon_g$.

The band gap of ScN, where its CBM is composed also of Sc $3d$ orbitals, deserves further discussion. Despite several experimental investigations [61,62,68,71], its fundamental indirect band gap from Γ to X is still not accurately determined and further accurate and direct determination of the band gap of ScN is still needed. The measured values range between 0.9 ± 0.1 eV [68] to 1.4 ± 0.2 eV [62]. Our calculated TB09 value of 0.75 eV improves considerably upon the LDA band gap and is closer to the lower experimental value and with the quasiparticle calculations starting from DFT data obtained using LDA (0.9 eV, 1.14 eV [40]) and optimized effective potential (OEP) approach (of 0.82 eV [40]). The OEP is equivalent to the exact exchange potential within the Kohn-Sham formalism of DFT [41]. On the other hand, our quasiparticle result based on TB09 (1.5 eV), screened-exchange LDA approach (1.58 eV) [70] and quasiparticle result based on HSE06 (1.36 eV) [71] support the upper experimental values. It was argued by Ref. 71 that these higher values can be attributed to an increase of the optical band gap due to the Burstein-Moss effect [69]. Moreover, the HSE06-GW calculations are found [71] to overestimate the *direct* band gaps of ScN at the Γ to X points, and the TB09-GW approach has the tendency of overestimating the band gap [72]. Bearing in mind that LDA calculations lead to a small negative band gap for ScN (see Table I), one can conclude that the TB09 functional improves considerably the band gap of ScN. This conclusion is in accord with the findings of Ref. 59, which shows that the band gaps of semiconducting transition-metal compounds are well described by the TB09 functional. This can be understood as a result of the p-d hybridization which leads to more extended CBM states compared to those of ScF_3 and YF_3.

Another specific effect resulted from the use of this functional is shown by the contraction ScF_3 valence-band width by 1 eV compared to LDA. A similar result was found in oxides and semiconductors, where TB09 strongly underestimates the valence- and conduction-band widths even more than LDA [72].

The inadequacy of the TB09 functional to properly describe the electronic structure of wide-band-gap insulators may be traced back to the observed instability of solutions obtained by the variational principle within the self-consistent scheme due to the high number of iterations needed to reach the converged results. A perturbative approach [73] to Tran-Blaha potential can give overall satisfactory results for a wide class of semiconductors and insulators. However, it can not be considered as the best method for describing the electron-electron interaction in semiconductors since it lacks an exchange-correlation energy whose functional derivative with respect to the electron density is equal to the v_x given

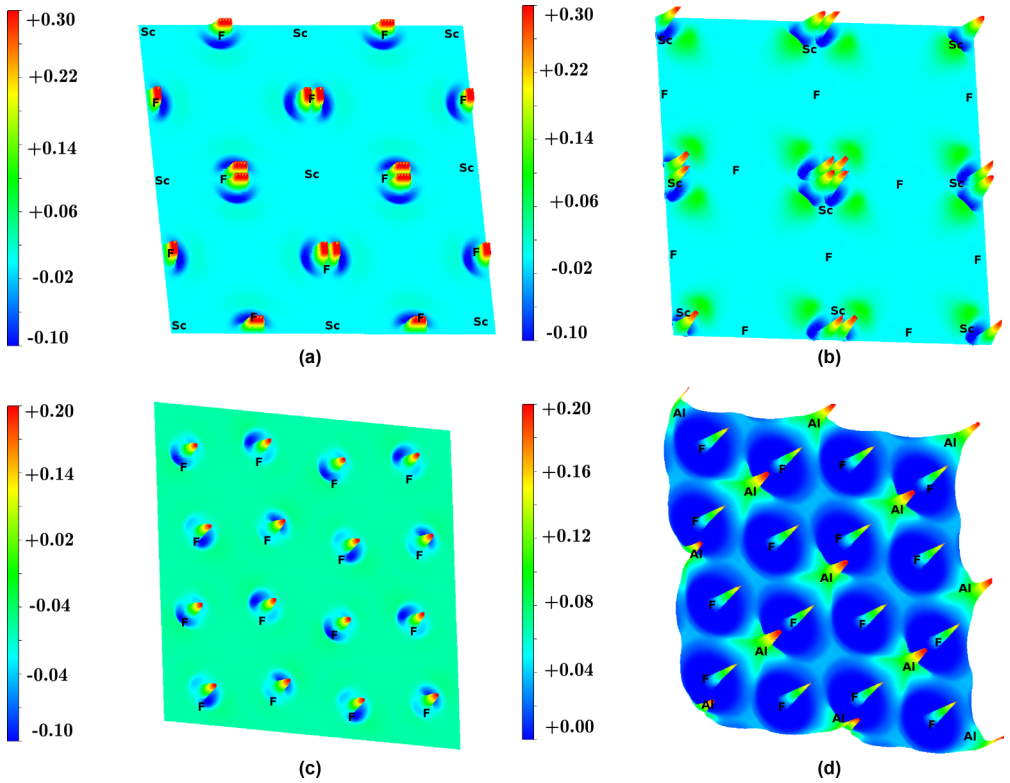

FIG. 4. (Color online) Calculated integrand of the TB09 correction to the LDA energies given by Eq. (32) for the VBM (left) and the CBM (right) and for both the cubic ScF_3 in the (100) plane (top) and for rhomboedric AlF_3 in the (110) plane (bottom).

by Eq. (1). This might prevent an accurate description of any energy related properties. Another drawback of this potential is that it suffers from the same derivative discontinuity as LDA and GGA.

Because of the lack of measured band gaps corresponding to the cubic phase of ScF_3, and the fact that the band gap calculated within the density functional theory is just the difference between the CBM and VBM energies, which is different from the quasiparticle band gap that is obtained from the difference of the ionization potential and the electronic affinity, we cannot therefore fully trust the results obtained by means of local or semilocal DFT functionals. Extending our study with hybrid functionals and MBPT will result in a more accurate electronic structure. This will enable us to compare our band structure for occupied states with the existing photoemission spectra of thin film ScF_3 [57,58].

The study of the electronic structure of small- and medium-band-gap materials employing the hybrid HSE06 is practical. However, this method underestimates the gap of wide-band-gap insulators [74]. One way of getting better agreement with experiment for wide-band-gap materials is to adjust empirically the mixing parameter α to take into account the nature of each material [75]. This approach is not pursued in the present study. We prefer to keep α equal to its default value to be able to compare on equal footing the results of different hybrid functionals.

Figure 5 displays the transition energies at various different high symmetry points of ScF_3 Brillouin zone, calculated within the three hybrid functionals (B3LYP, HSE06, PBE0) and with the GW approximation described above. The PBE0 functional gives the closest band gaps to the GW values. A use of a scissor shift can make the values of all functionals coincide with each other and with those of GW, except at the R point. A more detailed comparison of band gaps of ScF_3 is presented in Table II and will be discussed later.

Figure 6, shows a comparison of the ScF_3 density of states calculated within LDA, hybrid PBE0 functional, and the standard GW approximation. Notice that the calculation of the GW spectral function is computationally more complicated because the self-energy should be calculated for all frequencies and $\mathbf{k}$ points. Here, we used only the GW quasiparticle

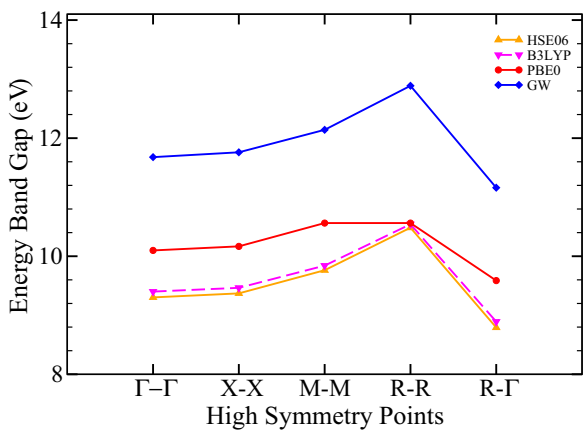

FIG. 5. (Color online) Calculated band-gap energies of ScF_3 with hybrid functionals compared to those of GW within the GN model.

TABLE II. Calculated band gaps of scandium trifluoride in eV with different exchange-correlation functionals and GW plasmon-pole models (PPm): GN stands for Godby-Needs, HL for Hybersten-Louie, VLH for von der Linden-Horsch, and FE for Farid-Engel.

	$E_G^{\Gamma\text{-}\Gamma}$	$E_G^{X\text{-}X}$	$E_G^{M\text{-}M}$	$E_G^{R\text{-}R}$	$E_G^{R\text{-}\Gamma}$
LDA	6.79	6.84	7.22	7.92	6.25
TB09	7.16	7.16	7.26	7.65	6.57
Hybrid-PBE0	10.10	10.17	10.56	11.29	9.59
Hybrid-HSE06	9.30	9.37	9.76	10.48	8.79
Hybrid-B3LYP	9.40	9.47	9.84	10.54	8.89
GW-PPm-GN	11.68	11.76	12.14	12.89	11.16
GW-PPm-HL	12.75	12.84	13.22	13.96	12.30
GW-PPm-VLH	12.15	12.27	12.79	13.67	11.62
GW-PPm-FE	11.76	11.86	12.30	13.10	11.23
scCOHSEX	14.78	14.88	15.39	16.22	14.31
GW@scCOHSEX	13.98	14.09	14.52	15.29	13.49

energies to determine the DOS. To facilitate the comparison, we set the VBM at the zero of energy. The figure shows that PBE0 did not improve the valence-band width, whereas GW increased it only slightly in agreement with photoemission [57,58]. However, PBE0 improved considerably the band gap by about 3.3 eV and GW produced a band gap of 11.16 eV, which will remain our best theoretical prediction. The large shift towards higher energies of the conduction states, either in PBE0 or GW, results therefore in a significant increase of the band gap compared to LDA.

The HL plasmon-pole model gives unphysical solutions manifested in the appearance of complex plasmon frequencies, which lead to imaginary plasmon-pole energies for some off-diagonal matrix elements [44]. As shown in Table II, the HL model gives band gaps larger than 12 eV for all high-symmetry points, which are the largest corrections to the LDA band structure. This is due to the overestimation of the plasmon frequency, which results in an underestimation of the Coulomb screening.

For scandium trifluoride, Table II shows that EF and GN models give similar corrections whereas the VLH model gives

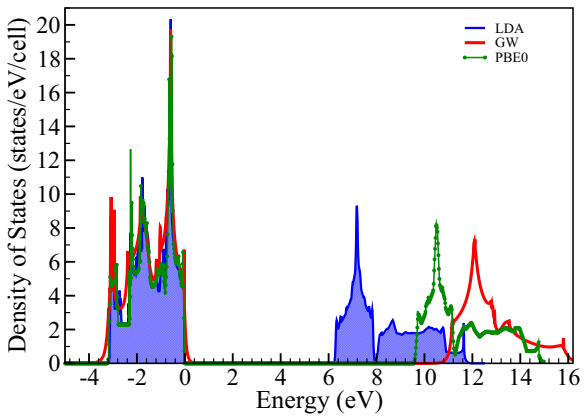

FIG. 6. (Color online) Density of states of ScF_3 obtained in the LDA, PBE0, and GW within the GN plasmon-pole model. The VBM is set to zero for a better comparison (the calculated LDA, PBE0, and GW values are, respectively, −1.63, −2.35, and −4.26 eV).

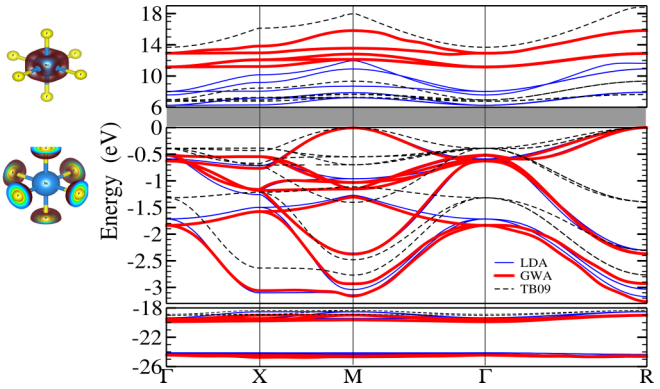

FIG. 7. (Color online) Calculated GW band structure of ScF_3 using the GN plasmon-pole model compared to LDA and TB09 results. The top of valence bands is set to zero to facilitate the comparison (the calculated LDA, TB09, and GW values are, respectively, −1.63, 1.00, and −4.26 eV). The LDA symmetry of the orbitals of the VBM (bottom left) and CBM (top left) are also shown.

slightly larger band gaps. Giving the time consuming in the f-sum rule models and the simplicity of the GN plasmon-pole model, which produces comparable results to those of EF model, it is the most appropriate and reliable of the four plasmon-pole models used in this study.

The GW band structure of ScF_3 is obtained within the Wannier function interpolation scheme. Figure 7 shows the quasiparticle GW band structure obtained using the GN plasmon-pole model. We set the top of valence bands to zero of energy to facilitate the comparison of GW, LDA, and TB09 results. The figure also shows the symmetry of VBM (bottom left) and CBM (top left). It is clear that the CBM is composed mainly of Sc e_g symmetry and is therefore very localized whereas VBM is composed of the $2p$ states of fluorine. It is interesting to notice that the lowest semicore states composed of F s states and Sc p states are shifted by only about 1 eV compared to LDA. However, the conduction-band width largely due to the Sc d states, is much reduced compared to LDA. This is due to the more localized nature of Sc d states within the GW approximation. The figure also shows that both the valence and the conduction-band widths within TB09 are much smaller than these of GW and LDA in disagreement with the valence-band width given by photoemission [57,58].

1. Effect of the starting point in the GW approximation

Accurate quasiparticle wave functions are key ingredients for calculating several properties of materials such as optical excitations, energy loss spectra, or x-ray absorption spectra. It is therefore quite important to choose a good starting point to conduct GW calculations. A simplified version of the GW approximation was proposed by Hedin [37], the so-called Coulomb hole screening exchange (COHSEX), which is restricted to the static screening and a summation over only occupied states with a Hermitian self-energy. We performed a self-consistent COHSEX calculation by updating both eigenvalues and eigenfunctions. This method tends to overestimate band gaps, as shown for ScF_3 (see Table II). Since doing the standard perturbative GW calculations starting from

TABLE III. Effective mass of ScF_3 in units of m_0 and the band-gap pressure coefficients in units of meV/kbar obtained from LDA and GN plasmon-pole model GW calculations.

	$m_h^{*\Gamma}$	$m_e^{*\Gamma}$	m_h^{*R}	m_e^{*R}	$a_p^{\Gamma-\Gamma}$	a_p^{R-R}	$a_p^{R-\Gamma}$
LDA	0.931	0.779	2.301	0.818	9.038	14.656	8.782
GW	0.881	0.784	2.281	0.833	10.778	16.665	10.644

self-consistent scCOHSEX gives a good agreement with the usual scGW [76], we studied the effect of this last method on the band gap of ScF_3 (see Table II). The resulting values with GW@scCOHSEX are smaller than those with the COHSEX only, a decrease of 0.8–0.9 eV is observed, but these values are still higher than the standard GW calculations using LDA as a starting point. This situation occurs always when handling the self-consistency of GW of both energies and wave functions. The self-consistency on GW leads to higher band gaps of materials.

2. Effective mass and hydrostatic pressure

In order to determine the effect of the GW approximation on the DFT curvature of bands, we made a comparison in Table III of the effective mass corresponding respectively to an electron in the bottom of conduction band and a hole in the top of valence band. The large effective mass of the top valence band observed at R point (larger than 2) is due to the localization of fluorine p states, whereas the cationic nature of conduction bands gives rise to a more dispersive band leading to low electron effective mass. The high value of the hole effective mass results in a low mobility in ScF_3.

Figure 8 displays the variation of the GW direct and indirect band gaps at Γ and R points. A compression of ScF_3 leads to an increase of band gaps, whereas a dilatation decreases them (a 5% increase in the cell volume results in 0.8% decrease in the band gap).

As shown in Fig. 8, the energy band gaps corresponding to Γ-Γ, R-R, and R-Γ transitions present a linear behavior as a function of the logarithmic scale of the relative unit cell volume. All calculated values of volume deformation potential are negative. The pressure coefficients are derived from the volume deformation potential using an empirical rule [77]. The GW method gives larger values than LDA coefficients because LDA underestimates the band gap pressure coefficients [78]. The variation of the ScF_3 band gaps with pressure are not available so our quasiparticle band gaps will remain a prediction.

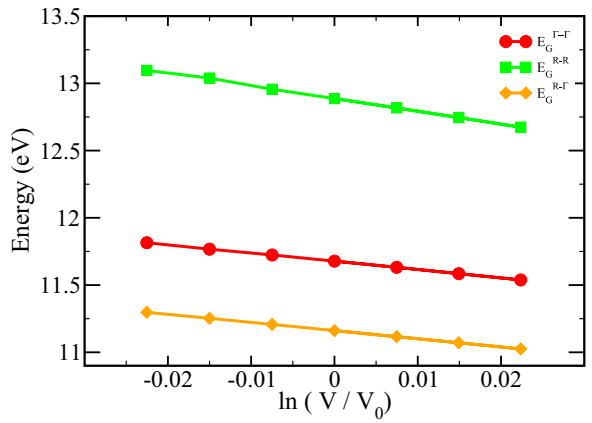

FIG. 8. (Color online) Variation of the GN plasmon-pole model GW band gaps of ScF_3 with respect to the change of the logarithm of the relative unit cell volume.

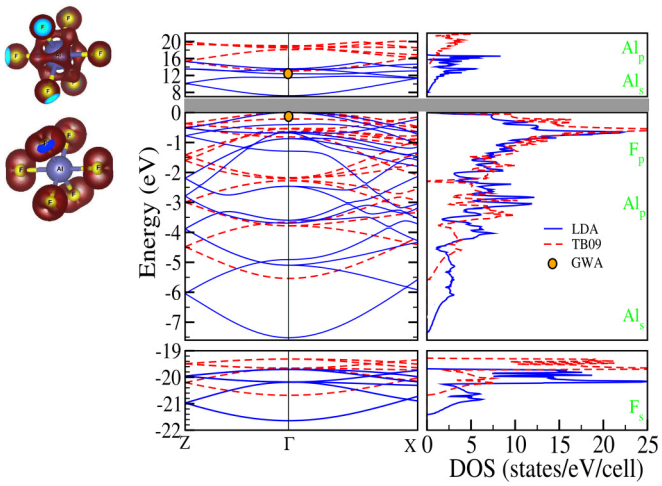

FIG. 9. (Color online) Calculated LDA and TB09 band structures and total density of states of AlF_3. The GW band gap is also displayed. The VBM is set to zero of energy to facilitate the comparison (the corresponding LDA, TB09, and GW VBM values are, respectively, −1.04, 0.91, and −3.79 eV). The LDA orbital symmetries of the VBM (bottom left) and the CBM (top left) are also shown as well as the fluorine s and p (F_s, F_p), aluminum s and p (Al_s, Al_p), and Sc d (Sc_d) (right) DOSs.

3. Electronic structure of AlF_3 and YF_3

AlF_3 crystallizes in the $R\bar{3}c$ structure [Fig. 1(b)], which is the same structure of ScF_3 in its high pressure phase. We choose to study this material using its rhombohedral coordinates rather than its hexagonal ones because in the latter one should use six units formula per unit cell. The aluminum atoms occupy the corners of the rhombohedron in the $R\bar{3}c$ structure, and the fluorine atoms are at the Wyckoff coordinates (0,0.42,0.25). The number of atoms per until cell is eight, which makes the GW calculation more time consuming.

Figure 9 displays the LDA and TB09 band structures and the total density of states of AlF_3. The VBM is set to zero of energy to facilitate the comparison. In all calculations, AlF_3 has a direct band gap at Γ point. The LDA band gap is 7.23 eV in agreement with that of Chen *et al.* [23], whereas the TB09 functional gives a large gap, reaching 13.06 eV, induced by an upward shift of the CBM and VBM by 7.78 and 1.94 eV, respectively (see also Table I). As shown in Table IV, the LDA band gap is much smaller than the one obtained within TB09. The large opening of the band gap with TB09 is expected, since this functional gives a better gaps for materials without d electrons (both the VBM and CBM are formed form sp-type bonding as shown in the left panel of Fig. 9). This is also confirmed by our GW result, which

TABLE IV. Calculated band gap of AlF_3 and YF_3 in eV using different exchange-correlation functionals and GW approximation within the GN plasmon-pole model compared to experiment.

Compound	LDA	TB09	PBE0	GW	Expt.
AlF_3	7.23	13.06	11.19	12.98	10.8[a]
YF_3	7.53	9.04	11.04	12.02	10.53[b] 12.5[c]

[a]Reference [66].
[b]Reference [80].
[c]Reference [15].

is in good agreement with TB09. The only drawback is that the TB09 valence-band width is drastically reduced by about 2 eV compared to our LDA and that of Ref. [23]. However, both the GW and TB09 gaps seem to be much higher than the experimental one by about 2.2 eV (see Table IV). This is at first surprising since the GW calculated gaps usually agree well with experiment. However, the experimental band gap presented here is obtained from AlF_3 deposited over SiO_2 and which consists of nanocrystallites embedded in an amorphous matrix. It is not clear from the paper whether AlF_3 is partly amorphous or not. It is not therefore clear whether this experimental band gap represents accurately the bulk band gap of AlF_3. Other experimental data using an energy loss spectrum of 500 eV electrons reflected from an AlF_3 thin film on Cu(100) gives a band gap of 10 ± 0.2 eV. This latter value is less accurate as their energy loss spectrum shows a large broadening into the gap region [79]. The value of the latter band gap should be expected to be larger. We believe therefore that the GW value of AlF_3 gap of about 13 eV will remain to be confirmed by future experimental data. The fact that PBE0 gives the closest band gap to GW approximation from the three studied hybrid functionals, we limit the study of AlF_3 by hybrid functionals to the PBE0 one in order to determine the effect of an additional amount of the exchange-correlation potential. Table IV shows that the PBE0 band gap is much reduced compared to GW and TB09 and only slightly increased with respect to the available experimental value. Like for ScF_3 PBE0, seems to underestimate the band gap by about 1.8 eV.

YF_3 has the $Pnma$ structure, as AlF_3 in the high-temperature phase [Fig. 1(c)]. The unit cell has 16 atoms, which makes the hybrid functional and GW calculations very time consuming. We therefore only produce the GW band gap for this material. The d electrons of yttrium are considered as valence electrons. Figure 10 displays the LDA and TB09 band structures and the total density of states of YF_3. In the LDA, it has an indirect band gap: the top of valence band is located at Z point and the bottom of the conduction band at Γ point. The LDA band gap is 7.53 eV and is in good agreement with the result of Vali [25]. However, the direct band gap at the Γ point is only slightly higher by about 0.05 eV since the top of the valence energy at Γ and Z differ only by 0.05 eV. When the exchange-correlation potential is calculated within TB09 functional, the band gap is direct at the Z point and is 9.04 eV. Here again the VBM at Z is only slightly higher than that at the Γ point by 0.2 eV. Unlike ScF_3, there is an increase by 1.51 eV when compared to the LDA value but is still much

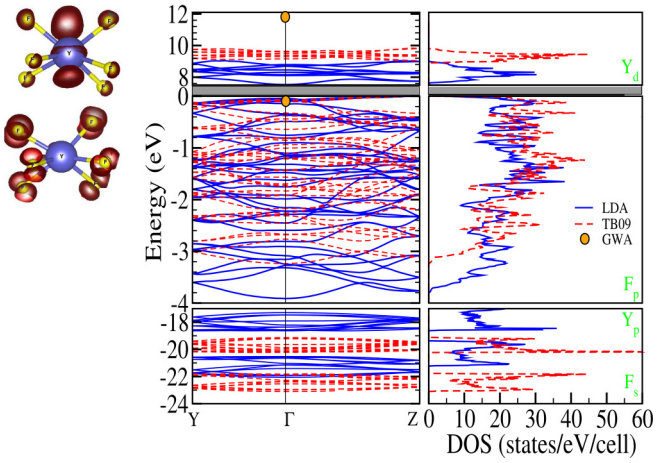

FIG. 10. (Color online) Same as the previous figure but for YF_3. The calculated LDA, TB09, and GW VBM values are, respectively, 3.34, 4.62, and -0.75 eV.

small than the lowest experimental value [80]. The hybrid PBE0 gives also a direct band gap at the Z point of 11.04 eV, which is between the two experimental values [15,80]. This PBE0 gap is, however, only 0.05 eV larger than the direct band gap at the Γ point. The GW band gap value is 12.02 eV and is higher than that of PBE0 and seems to agree more with the experimental value of Pankratov and coworkers [15]. The LDA band width of 3.8 eV is also in agreement with the calculation of Vali [25] and valence-band full width at half-maximum of 3.5 eV obtained by x-ray photoelectron spectroscopy [81]. Note that the TB09 band width is much smaller compared to experiment (see Fig. 10). The LDA calculated binding energy of the fluorine $2s$ and Y $4p$ (see Fig. 10) are 21 and 18 eV, respectively, and are also in good agreement with the corresponding experimental results [81] of 21.5 and 17.6 eV, determined with respect to the binding energy of fluorine $2p$ states.

IV. CONCLUSION

The electronic structure for scandium trifluoride is performed in the framework of various DFT hybrid functionals and GW method using four different plasmon-pole models. A failure of the Tran-Blaha TB09 functional to describe appropriately the band gap of ScF_3 was shown and justified. A comparison between three hybrid functionals and GW results for wide band gap insulators was investigated. Relying on these observations, we calculated the electronic structure of YF_3 and AlF_3 with TB09, the hybrid PBE0 functional and GW approximation. The performance of TB09 to the three considered trifluorides differs according to the presence/absence of d electrons, and its failure in the case of ScF_3 and YF_3 is mainly due to high localization of the conduction band minimum states which have almost pure d character. The TB09 valence-band width seems also to be excessively localized compared to those obtained within LDA, hybrid functionals, or GW. As a byproduct, a detailed comparison of the different

GW plasmon-pole models presenting the dynamical effects of the screened electronic interaction leads to the conclusion that the GN plasmon-pole model is the simplest model for the description of the electronic structure of wide-band-gap materials.

ACKNOWLEDGMENTS

This work was performed using HPC resources from GENCI/CINES allocation x2015095066 and Strasbourg HPC mesocenter. One of us N.M. thanks gratefully the Yarmouk University for constant financial support.

[1] J. Ge, L. Zhao, H. Guo, Z. Lan, L. Chang, Y. Li, and H. Yu, Phys. Chem. Chem. Phys. **15**, 17281 (2013).
[2] L. Liu, M. Zhou, L. Yi, H. Guo, J. Tan, H. Shu, X. Yang, Z. Yang, and X. Wang, J. Mater. Chem. **22**, 17539 (2012).
[3] C. Li and J. Lin, J. Mater. Chem. **20**, 6831 (2010).
[4] L. Chong, J. Zou, X. Zeng, and W. Ding, J. Mater. Chem. A **1**, 3983 (2013).
[5] M. A. Poulain, M. I. Poulain, and M. Matecki, Mater. Res. Bull. **17**, 661 (1982).
[6] P. Daniel, A. Bulou, M. Rousseau, J. Nouet, and M. Leblanc, Phys. Rev. B **42**, 10545 (1990).
[7] C. W. Li, X. Tang, J. A. Muñoz, J. B. Keith, S. J. Tracy, D. L. Abernathy, and B. Fultz, Phys. Rev. Lett. **107**, 195504 (2011).
[8] B. K. Greve, K. L. Martin, P. L. Lee, P. J. Chupas, K. W. Chapman, and A. P. Wilkinson, J. Am. Chem. Soc. **132**, 15496 (2010).
[9] K. S. Aleksandrov, V. N. Voronov, A. N. Vtyurin, S. V. Goryaĭnov, N. G. Zamkova, V. I. Zinenko, and A. S. Krylov, J. Exp. Theor. Phys. **94**, 977 (2002).
[10] L. Han, Y. Wang, L. Guo, L. Zhao, and Y. Tao, Nanoscale **6**, 5907 (2014).
[11] C. R. Morelock, B. K. Greve, L. C. Gallington, K. W. Chapman, and A. P. Wilkinson, J. Appl. Phys. **114**, 213501 (2013).
[12] A. P. W. Cody, R. Morelock, and Leighanne C. Gallington, J. Solid State Chem. **222**, 96 (2015).
[13] C. R. Morelock, L. C. Gallington, and A. P. Wilkinson, Chem. Mater. **26**, 1936 (2014).
[14] P. S. Peijzel, R. T. Wegh, A. Meijerink, J. Hls, and R.-J. Lamminmki, Opt. Commun. **204**, 195 (2002).
[15] V. Pankratov, M. Kirm, and H. von Seggern, J. Lumin. **113**, 143 (2005).
[16] A. C. E Sarantopoulou and Z. Kollia, Opt.l Mater. **18**, 23 (2001).
[17] C. Gong, Q. Li, R. Liu, Y. Hou, J. Wang, X. Dong, B. Liu, X. Yang, Z. Yao, X. Tan, D. Li, J. Liu, Z. Chen, B. Zou, T. Cui, and B. Liu, Phys. Chem. Chem. Phys. **15**, 19925 (2013).
[18] C. Michel, J.-M. Moreau, and W. J. James, Acta Crystallogr. B **27**, 501 (1971).
[19] P. Daniel, A. Bulou, M. Rousseau, J. Nouet, J. L. Fourquet, M. Leblanc, and R. Burriel, J. Phys. Condens. Matter **2**, 5663 (1990).
[20] C. R. Morelock, J. C. Hancock, and A. P. Wilkinson, J. Solid State Chem. **219**, 143 (2014).
[21] P. J. Chupas, S. Chaudhuri, J. C. Hanson, X. Qiu, P. L. Lee, S. D. Shastri, S. J. L. Billinge, and C. P. Grey, J. Am. Chem. Soc. **126**, 4756 (2004).
[22] S. Chaudhuri, P. Chupas, B. J. Morgan, P. A. Madden, and C. P. Grey, Phys. Chem. Chem. Phys. **8**, 5045 (2006).
[23] Y.-R. Chen, V. Perebeinos, and P. B. Allen, Phys. Rev. B **69**, 054109 (2004).
[24] F. Tran and P. Blaha, Phys. Rev. Lett. **102**, 226401 (2009).
[25] R. Vali, Comput. Mater. Sci. **50**, 2391 (2011).
[26] P. Hohenberg and W. Kohn, Phys. Rev. **136**, B864 (1964).
[27] W. Kohn and L. J. Sham, Phys. Rev. **140**, A1133 (1965).
[28] A. D. Becke and M. R. Roussel, Phys. Rev. A **39**, 3761 (1989).
[29] A. D. Becke, J. Chem. Phys. **98**, 1372 (1993).
[30] A. D. Becke, J. Chem. Phys. **98**, 5648 (1993).
[31] C. Adamo and V. Barone, J. Chem. Phys. **110**, 6158 (1999).
[32] J. Heyd, G. E. Scuseria, and M. Ernzerhof, J. Chem. Phys. **118**, 8207 (2003).
[33] W. Chen and A. Pasquarello, Phys. Rev. B **86**, 035134 (2012).
[34] J. E. Moussa, P. A. Schultz, and J. R. Chelikowsky, J. Chem. Phys. **136**, 204117 (2012).
[35] M. A. L. Marques, J. Vidal, M. J. T. Oliveira, L. Reining, and S. Botti, Phys. Rev. B **83**, 035119 (2011).
[36] C. Franchini, J. Phys. Condens. Matter **26**, 253202 (2014).
[37] L. Hedin, Phys. Rev. **139**, A796 (1965).
[38] M. S. Hybertsen and S. G. Louie, Phys. Rev. B **34**, 5390 (1986).
[39] J.-L. Li, G.-M. Rignanese, E. K. Chang, X. Blase, and S. G. Louie, Phys. Rev. B **66**, 035102 (2002).
[40] A. Qteish, P. Rinke, M. Scheffler, and J. Neugebauer, Phys. Rev. B **74**, 245208 (2006).
[41] P. Rinke, A. Qteish, J. Neugebauer, C. Freysoldt, and M. Scheffler, New J. Phys. **7**, 126 (2005).
[42] W. G. Aulbur, L. Jönsson, and J. W. Wilkins, *Solid State Physics*, edited by H. Ehrenreich and F. Spaepen (Academic Press, New York, 2000), pp. 1–218.
[43] R. W. Godby and R. J. Needs, Phys. Rev. Lett. **62**, 1169 (1989).
[44] W. von der Linden and P. Horsch, Phys. Rev. B **37**, 8351 (1988).
[45] G. E. Engel and B. Farid, Phys. Rev. B **47**, 15931 (1993).
[46] X. Gonze, B. Amadon, P.-M. Anglade, J.-M. Beuken, F. Bottin, P. Boulanger, F. Bruneval, D. Caliste, R. Caracas, M. Cote, T. Deutsch, L. Genovese, P. Ghosez, M. Giantomassi, S. Goedecker, D. Hamann, P. Hermet, F. Jollet, G. Jomard, S. Leroux, M. Mancini, S. Mazevet, M. Oliveira, G. Onida, Y. Pouillon, T. Rangel, G.-M. Rignanese, D. Sangalli, R. Shaltaf, M. Torrent, M. Verstraete, G. Zerah, and J. Zwanziger, Comput. Phys. Commun. **180**, 2582 (2009).
[47] A. A. Mostofi, J. R. Yates, Y.-S. Lee, I. Souza, D. Vanderbilt, and N. Marzari, Comput. Phys. Commun. **178**, 685 (2008).
[48] P. Giannozzi, S. Baroni, N. Bonini, M. Calandra, R. Car, C. Cavazzoni, D. Ceresoli, G. L. Chiarotti, M. Cococcioni, I. Dabo, A. Dal Corso, S. de Gironcoli, S. Fabris, G. Fratesi, R. Gebauer, U. Gerstmann, C. Gougoussis, A. Kokalj, M. Lazzeri, L. Martin-Samos, N. Marzari, F. Mauri, R. Mazzarello, S. Paolini, A. Pasquarello, L. Paulatto, C. Sbraccia, S. Scandolo, G. Sclauzero, A. P. Seitsonen, A. Smogunov, P. Umari, and R. M. Wentzcovitch, J. Phys. Condens. Matter **21**, 395502 (2009).
[49] N. Troullier and J. L. Martins, Phys. Rev. B **43**, 1993 (1991).

[50] M. J. Oliveira and F. Nogueira, Comput. Phys. Commun. **178**, 524 (2008).
[51] H. J. Monkhorst and J. D. Pack, Phys. Rev. B **13**, 5188 (1976).
[52] F. Gygi and A. Baldereschi, Phys. Rev. B **34**, 4405 (1986).
[53] J. Spencer and A. Alavi, Phys. Rev. B **77**, 193110 (2008).
[54] F. Bruneval and X. Gonze, Phys. Rev. B **78**, 085125 (2008).
[55] K. S. Aleksandrov, V. N. Voronov, A. N. Vtyurin, A. S. Krylov, M. S. Molokeev, M. S. Pavlovskiĭ, S. V. Goryaĭnov, A. Yu. Likhachev, and A. I. Ancharov, Phys. Solid State, **51**, 810 (2009).
[56] P. E. Blöchl, O. Jepsen, and O. K. Andersen, Phys. Rev. B **49**, 16223 (1994).
[57] M. Umeda, Y. Tezuka, S. Shin, and A. Yagishita, Phys. Rev. B **53**, 1783 (1996).
[58] S. Shin, Y. Tezuka, T. Ishii, and Y. Ueda, Solid State Commun. **87**, 1051 (1993).
[59] D. Koller, F. Tran, and P. Blaha, Phys. Rev. B **85**, 155109 (2012).
[60] D. Koller, F. Tran, and P. Blaha, Phys. Rev. B **83**, 195134 (2011).
[61] D. Gall, M. Städele, K. Järrendahl, I. Petrov, P. Desjardins, R. T. Haasch, T.-Y. Lee, and J. E. Greene, Phys. Rev. B **63**, 125119 (2001).
[62] S. W. King, R. F. Davis, and R. J. Nemanich, J. Vac. Sci. Technol. A **32**, 061504 (2014).
[63] C. Kittel, *Introduction to Solid State Physics*, 8th ed. (John Wiley & Sons, New York, 2004).
[64] M. Piacentini, D. W. Lynch, and C. G. Olson, Phys. Rev. B **13**, 5530 (1976).
[65] G. W. Rubloff, Phys. Rev. B **5**, 662 (1972).
[66] D. Koenig, R. Scholz, D. R. T. Zahn, and G. Ebest, J. Appl. Phys. **97**, 093707 (2005).
[67] D. J. Singh, Phys. Rev. B **82**, 205102 (2010).
[68] H. A. Al-Brithen, A. R. Smith, and D. Gall, Phys. Rev. B **70**, 045303 (2004).
[69] P. Rinke, M. Scheffler, A. Qteish, M. Winkelnkemper, D. Bimberg, and J. Neugebauer, Appl. Phys. Lett. **89**, 161919 (2006).
[70] C. Stampfl, W. Mannstadt, R. Asahi, and A. J. Freeman, Phys. Rev. B **63**, 155106 (2001).
[71] R. Deng, B. D. Ozsdolay, P. Y. Zheng, S. V. Khare, and D. Gall, Phys. Rev. B **91**, 045104 (2015).
[72] D. Waroquiers, A. Lherbier, A. Miglio, M. Stankovski, S. Poncé, M. J. T. Oliveira, M. Giantomassi, G.-M. Rignanese, and X. Gonze, Phys. Rev. B **87**, 075121 (2013).
[73] H. Jiang, J. Chem. Phys. **138**, 134115 (2013).
[74] Y.-i. Matsushita, K. Nakamura, and A. Oshiyama, Phys. Rev. B **84**, 075205 (2011).
[75] D. Koller, P. Blaha, and F. Tran, J. Phys. Condens. Matter **25**, 435503 (2013).
[76] F. Bruneval, N. Vast, and L. Reining, Phys. Rev. B **74**, 045102 (2006).
[77] S.-H. Wei and A. Zunger, Phys. Rev. B **60**, 5404 (1999).
[78] N. E. Christensen, Phys. Rev. B **30**, 5753 (1984).
[79] G. Ruano, R. Vidal, J. Ferrn, and R. Baragiola, Surf. Sci. **605**, 1807 (2011).
[80] J. Krupa and M. Queffelec, J. Alloys Compd. **250**, 287 (1997).
[81] N. Kirikova, J. Krupa, V. Makhov, and C. Severac, J. Electron Spectrosc. Relat. Phenom. **122**, 85 (2002).